RSC Advances

ROYAL SOCIETY OF CHEMISTRY

www.rsc.org/advances

Journal Name

ARTICLE

Enhancing Thermal Transport Efficiency in Carbon Composites Using Nanospacers

Received 00th January 20xx,
Accepted 00th January 20xx

DOI: 10.1039/x0xx00000x

www.rsc.org/

Chien-Te Hsieh*, Yu-Fu Chen, Cheng-En Lee, Shi-Hong Juang, Zih-Wei Lin, Mohammad Mahmudul Huq

Improved thermal transport efficiency of carbon-based composites has been achieved by inserting metallic spacers within the temperature range of 50-150 °C. Al_2O_3, Ni, and SnO nano-particles are used as nanospacers in the graphite-like thin films, forming well-developed carbon framework. The composites show 42.5-57.7% increase in thermal conductivity (*k*), as compared with the pristine carbon. Among all the samples Al-inserted carbon composites exhibited the highest *k* value of 1128 W/m K at 50°C. The metallic nanopowders serve not only as filler but also as connective points for creating additional path for the heat conduction, leading to highly-efficient thermal diffusion. The apparent *k* value is found to be an increasing function of electrical conductivity, revealing that the conduction of free electrons is analogous to the thermal transport. The present work provided useful information concerning the thermal conduction and heat dissipation efficiencies of carbon-based composites, benefiting the design of thermal devices, e.g., heat sink and heat exchanger.

Introduction

Thermal management devices such as heat exchangers and heat sinks are ubiquitous, and the overall efficiency, cost and size of the heat exchanger are the key factors in evaluating their performance.[1] It is generally recognized that carbonaceous materials possess a number of favourable characteristics, making them ideal construction materials for some operating environments. This is because carbon-based materials are inert, stable within a wide temperature range, and resistant to most common corrosive reagents.[1] Furthermore, carbons usually have low density (e.g., graphite with a low density of approximately 2.2 g/cm^3), suitably complementing for compact and lightweight applications.[2] For various practical applications, several types of carbon materials including synthetic diamond, adsorbent carbon, coke, graphitic carbon, carbon fibers, and carbon black, have been created by researchers and engineers.[3] Among the carbon materials, graphite-like carbons have been reported to have an extremely high thermal conductivity (*k*) parallel to the graphite layers, which could achieve a *k* value of as high as 4180 W/m k for a single crystal, based on the molecular dynamics simulations.[4,5] Such high *k* value has attracted many scientists and researchers to consider graphite as engineering materials for high-performance heat sinks and heat exchangers.

Accordingly, a number of efforts have been made to study the thermal transport performance of carbon-based heat sinks such as preferred-oriented graphite blocks (*k* = 522 W/m K),[2] graphite blocks (*k* = 704 W/m K),[4] flake graphite/polymer composites with carbon fillers (*k* = ~525 W/m K),[6] multilayer graphene architecture (*k* = 112 W/m K),[7] Cu-graphene heterogeneous films (*k* = 373 W/m K).[8] However, these *k* values are still far away from the theoretical one, i.e., 4180 W/m K. This difference mainly originates from the efficiency of thermal transport that is strongly influenced by the presence of intrinsic defects, point defects, topological defects, edge termination, surface roughness, surface heterogeneity, and voids or cavities in carbon-based structures.[9] The blockage of thermal transport induces an increased resistance to transport of collective vibrations or phonons responsible for heat conduction in various materials.[10,11] Thus, a unique design of carbon-based architectures could effectively enhance the thermal conduction efficiency of heat sinks, favourable for engineering applications.

One of the efficient design strategies involves inserting metal oxide nanoparticles in carbon structures, creating a well-developed conductive framework. In the present work, we employ three types of metal nanoparticles, aluminium (Al, *k* = 205 W/m K), nickel (Ni, *k* = 91 W/m K) and tin (Sn, *k* = 67 W/m K), as spacers in the carbon black layers. The *k* values of metal particles are far superior to that of air pocket, which has a *k* value of 0.024 W/m K. The inserted metal particulates are believed to fill with the voids and cavities of porous carbon layers after the compression treatment. The thermal conduction properties of carbon composites were systematically investigated. The present work would shed some lights on (i) the influence of metal nanospacers on the *k* values of carbon-based heat sinks and (ii) the relationship between *k* value and electrical conductivity (σ) in the heat sinks.

[a] Department of Chemical Engineering and Materials Science, Yuan Ze University, Taoyuan 32003, Taiwan. E-mail: cthsieh@saturn.yzu.edu.tw. Tel.: 886-3-4638800 ext.2577; Fax: 886-3-4559373.

Experimental

Fabrication of metal-coated carbon composites

An artificial carbon black powder (Type: KS-4) were purchased from Taiwan Maxwave Co. The carbon black powders had an average particle size of 2.4 mm, and the apparent density of pristine carbon layer is approximately 0.72 g/cm^3. Three types of metal nanopowders, Al, Ni, and Sn, were supplied from HCH instrument, JT-Baker, and Sigma-Aldrich, respectively. All of them are reagent grade with high purity of > 99.8%. First, the carbon black powders (2.25 g) were homogeneously dispersed in isopropanol at ambient temperature. Afterward, metal nanopowders (0.15 g) were slowly added into the carbon slurry. The slurries were then placed in a high-performance homogenizer (IKA, Model T25, Germany). The homogenizer was equipped with a rotor-stator generator, served as a centrifugal pump to re-circulate isopropanol and solids in liquid phase. The homogenizing dispersion process was performed with a high rotation speed of 24,000 rpm for 0.5 h, thus, producing the uniform slurries. Finally, the carbon composites were dried at 120°C in a vacuum oven overnight.

For thermal transport measurement, the carbon composites were well coated over Cu foils with a thickness of 10 μm. The carbon composites were well mixed with a binder (poly-vinylidenefluoride) with the weight ratio of 75:25 in N-methyl pyrrolidinone (NMP) solvent to form the carbon slurries. The slurries were then blended with a three-dimensional mixer by using zirconia balls for 0.5 h. The as-prepared slurries were pasted on the Cu foil substrates with a doctor blade, followed by evaporating NMP solvent with a blow dryer. After that, the as-prepared carbon layers were dried at 120°C in a vacuum oven overnight. The carbon sheets were then pressed under a pressure of ~200 kg cm^{-2}. Finally, the carbon-based sheets were carefully cut into an area of 20 × 50 mm for thermal transport measurement. For identification, herein four types of samples were designated as C, CAl, CNi, and CSn, according to pristine carbon black, Al-, Ni-, and Sn-coated carbon composites, respectively.

Characterization of metal-coated carbon composites

Micro-structural observation of metal-coated carbon composites was carried out by Field-emission scanning electron microscopy (FE-SEM; JEOL JSM-6701F) and transmission electron microscopy (TEM; JEOL, JEM-2100). An X-ray diffraction (XRD; Shimadzu Labx XRD-6000) spectroscope, equipped with Cu-Kα radiation emitter, was adopted to examine the crystalline structure of carbon composites. An automated adsorption apparatus (Micromeritics, ASAP 2020) was used for analyzing the surface characteristics of the carbon composites, using N_2 physisorption at -196°C. Specific surface areas and pore size distributions of the carbons were analyzed with the application of the Brunauer-Emmett-Teller (BET) and the Barrett-Joyner-Halenda (BJH) equations, respectively. The crystalline structure of carbon composites was characterized by using Raman spectroscope (Renishaw Micro-Raman spectrometer). The weight percentage of metallic nanopowders on the carbon matrix was determined by using thermogravimetric analyzer (TGA, Perkin Elmer TA7). The TGA analysis was carried out under a steady air flow with a ramping rate of 10 °C/min within the temperature range of 50−1000°C.

One home-made system for evaluating in-plane *k* value of heat sinks has been reported in our pervious study.[10] The schematic diagram concerning the evaluation of *k* value was illustrated in Fig. 1. High-purity (i.e., 99.95%) Cu foils with different dimensions served as references. Before each experimental run, the calibration curves of operating temperature versus heat transfer from an electrical resistance heater were obtained. The test temperatures lie in the region of 50–150°C, suited for the thermal management of chips for consumer electronics. All heat sinks were insulated with heat-preservation cotton to avoid any heat dissipation. We employed one thermal imager to detect the surface temperature distribution of heat sink. The temperature reading was monitored and recorded by using five thermal couples (K-type, accuracy: ±0.1°C), one on the heater, three on the heat sink, and one for measuring the ambient temperature. The apparent *k* values of heat sink could be determined by using the Fourier's law, based on one-dimensional heat conduction.[13] The *k* values were obtained by comparing the temperature drops across the heat sink, followed by the calculations of the Fourier's law. We adopted a four-point probe tester to measure electrical conductance of heat sinks at ambient temperature. Herein each reading was averaged from four σ values at different locations of heat sinks.

Results and discussion

The physical structure of original carbon black has been investigated using FE-SEM, as shown in Fig. 2. It can be seen that the pristine C sample is composed of a number of flat graphite sheets, voids and cavities, allowing air layer trapped inside the carbon structure. The thickness of pristine carbon-based layer is approximately 40 μm after the compression treatment. Figs. 2(a), 2(b), and 2(c) depict top-view FE-SEM micrographs for CAl, CNi, and CSn samples, respectively. The photos clearly illustrate that there are a number of metal nanopowders onto the surface of carbon black after the metal mixing and coating process. This observation proves that the homogenizing method is an effective process that brings about well dispersion of metal nanopowders over the carbon surface through shear, impact, collision, and cavitation in liquid phase.

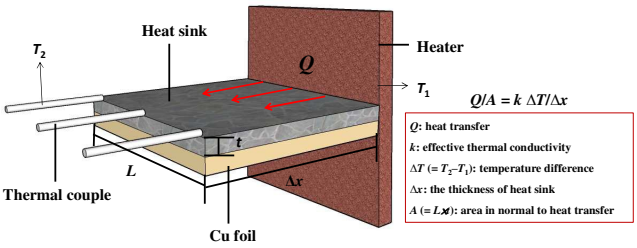

Fig. 1 The schematic diagrams of experimental setup for calculating effective thermal conductivity of carbon-based heat sinks, using Fourier's law.

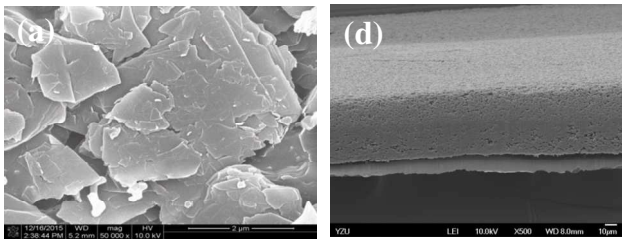

Fig. 2 (a) Top- and (b) cross-sectional views of FE-SEM images for pristine carbon black sample.

The cross-sectional FE-SEM micrographs for all heat sinks are presented in Fig. 3(d)–(f). Herein the compression ratio was set at 40%, showing dense carbon-based layers adhered to the Cu foils. The thickness of carbon-based layers ranges from 24 to 43 μm after the compression treatment. Basically, the composite files possess a smooth and flat surface, as observed from the cross-sectional view inspection. This result indicates that the carbon composites become more compact than original ones, inducing more thermal conductive channels and less thermal resistivity.

Porous characteristics of different carbon composites were determined from the data of N_2 adsorption isotherms. For comparison, the CSn sample displays a BET surface area of 74.1 m^2/g, higher than the CNi and CAl samples with low surface areas of 32.7 and 30.2 m^2/g, respectively. The BJH method was adopted to analyze the pore size distribution of all carbon composites, as depicted in Figure 4. The figure reveals that these carbon samples are mainly mesoporous, exhibiting a resemble pore size distribution. The major peaks of CAl, CNi, and CSn sample center at *ca*. 20–30 nm. It can be found that the CSn sample displays higher pore volume as compared to the others, confirming higher porosity for air trapping in the CSn sample. The porosity in the carbon composites possibly originates from inner cavities, interstitial channels, and the aggregate's outer surfaces. Next, we expect that the compact composite layers are able to reduce the possibility of phonon-boundary scattering. HR-TEM was employed to observe the micro-structures of CAl, CNi, and CSn samples, as illustrated in Fig. 5(a)–(c). It can be seen that three types of metal nanopowders are decorated onto the surface of carbon black, forming hierarchical carbon-based composites. The Al, Ni, and Sn nanopowders show a random distribution over the carbon matrix. It is worth noting that the metallic nanopowders have three different morphologies: cluster (Al), rod (Ni), and sphere (Sn).

XRD technique was adopted to examine the crystalline structures of carbon samples, as shown in Fig. 6. Typical XRD patterns of different carbon samples reveal that all samples possess a characteristic peak (002) of graphite at approximately 26.2°. Based on the analysis of Bragg's equation, the interlayer distance (d_{002}) is approximately 0.340 nm, very close to highly-oriented graphite carbon (i.e., 0.335 nm).[13] It has also confirmed the presence of Al_2O_3, Ni, and SnO crystals in the CAl, CNi, and CSn samples, respectively. According to the JCPDS standard patterns, the Al_2O_3, Ni, and SnO nanopowders are indexed as trigonal (a = 4.780 Å and c = 1.299 Å), layered (a = 3.802 Å and c = 4.836 Å), and face-centered cube (a = 3.520 Å) crystalline structures, respectively.

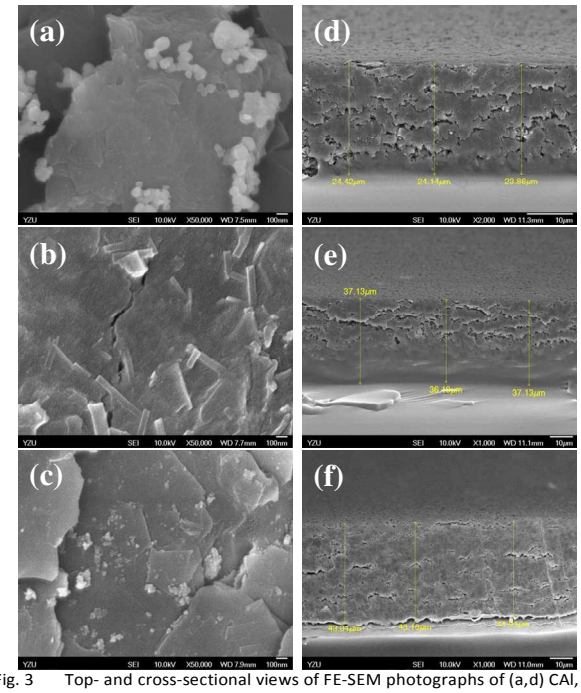

Fig. 3 Top- and cross-sectional views of FE-SEM photographs of (a,d) CAl, (b,e) CNi, and (c,f) CSn samples.

This result reflects that the Al and Sn nanopowders are prone to be mostly oxidized by air while preparing the composite layers during the homogenizing or coating process.

To inspect the influence of metal insertion on the crystalline structure, the degree of graphitization of carbon-based composites is further characterized by Raman spectroscopy, as shown in Fig. 7.

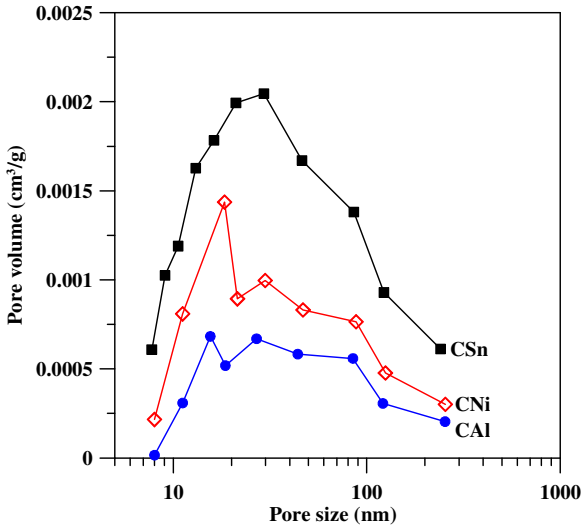

Fig. 4 Pore size distributions of different carbon composites.

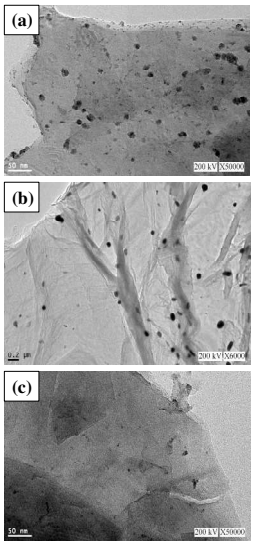

Fig. 5 HR-TEM photographs of (a) CAl, (b) CNi, and (c) CSn samples.

Herein these spectra display Raman signatures of various carbon composites within the region between 1000 and 2000 cm^{-1}. Two main Raman bands at *ca*. 1350 and 1580 cm^{-1}, assigned to the D- and G-band peaks appear in all spectra, respectively. The *G*-band can be ascribed to the vibration of sp^2-bonded carbon atoms in a two-dimensional hexagonal lattice, while the *D*-band either originates from the vibration of carbon atoms with dangling bonds in crystal lattice plane terminations of disordered graphite, or from the defects in curved graphene sheets.[14] It is generally recognized that the intensity ratio of the *D*- to *G*-band, I_D/I_G, can be considered as an important indicator in evaluating the graphitic quality of carbon materials.[14,15] The I_D/I_G ratios of C, CAl, CNi, and CSn are 0.17, 0.26, 0.34, and 0.40, respectively. The increased I_D/I_G ratio can be attributed to the fact that the metallic nanopowders are prone to attach to the basal plane or edge of graphite, partially accompanying the decoration of heteroatoms and thus producing amorphous carbons through the high-performance homogenizing route.

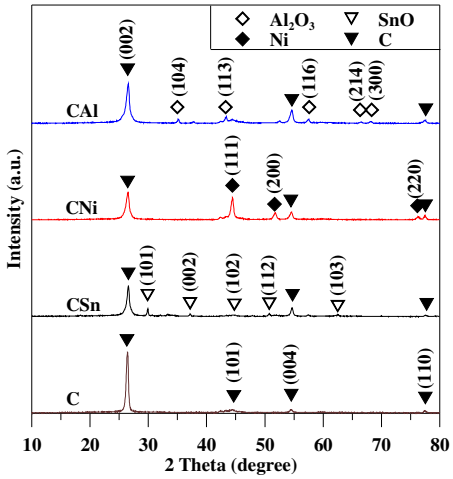

Fig. 6 Typical XRD patterns of pristine C, CAl, CNi, and CSn samples.

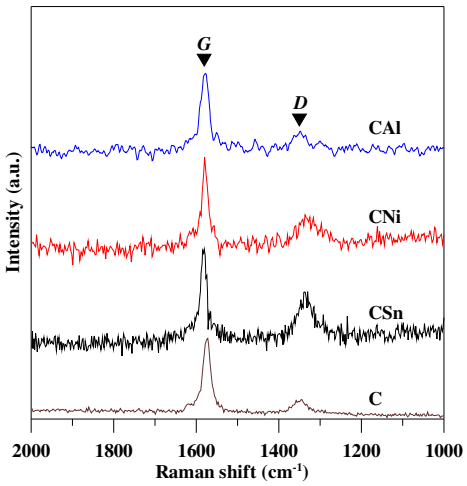

Fig. 7 Raman spectra of pristine C, CAl, CNi, and CSn samples

Fig. 8 illustrates the TGA weight-loss curves obtained by thermally treating the carbon composites in air at a heating rate of 10 °C/min. It can be found that the TGA curves show an apparent weight loss within the temperature range from 700° to 900°C. This weight loss mainly comes from the gasification of carbon black in the presence of oxygen gas. The residual percentages are 93.6, 92.0, and 92.3 % for CAl, CNi, and CSn samples, respectively. The results indicate that the weight loading of metallic nanopowders in the carbon composites is approximately 6.4–8.0 %, in good agreement with the dose of various powders during the material preparation.

The variation of *k* value with operating temperature for various carbon composites is depicted in Fig. 9. The figure clearly reveals that the *k* value is a decreasing function of temperature within the entire temperature region of 50–150°C. This can be attributed to an increase in phonon population with higher energy states, leading to an increase in phonon scattering.[9] This phenomenon concerning the phonon scattering becomes more evident at high temperature, unfavorable for thermal transport in conductive carbon composites.

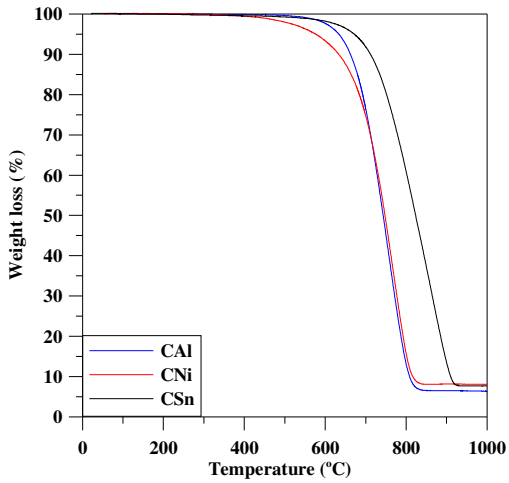

Fig. 8 TGA weight-loss curves of CAl, CNi, and CSn samples.

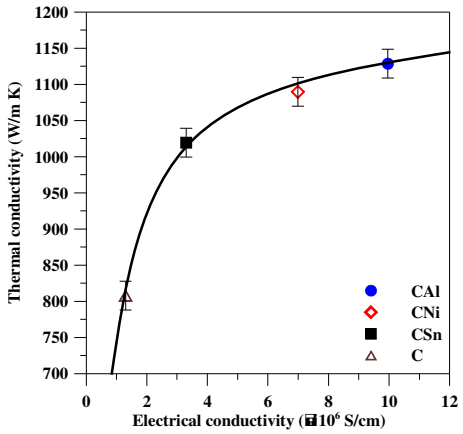

Fig. 9 In-plane thermal conductivity as a function of operating temperature for all carbon samples.

Herein it is noticed that the decreasing function is incompatible with the Umklapp phonon-phonon scattering that displays approximately $1/T$ temperature dependence.[16] In comparison, the *k* value at 50°C has an order as: CAl (1128 W/m K) > CNi (1089 W/m K) > CSn (1019 W/m K) > C (715 W/m K). This result reflects that the insertion of metallic nanopowders delivers the positive effect on the improved thermal transport efficiency in the carbon architectures. An increase of 42.5–57.7 % in the improved *k* value can be achieved after the introduction of metallic spacers. It is generally recognized that the thermal conduction is mainly dominated by phonon-boundary scattering, strongly affected by the lattice vibration and phonon mean free path in basal planes of carbon.[17,18] The pristine graphite-like layer (i.e., C sample) consists of a large number of voids and cavities that impart more thermal transport resistivity, raising the possibility for the phonon-boundary scattering. In the other words, the mean free path of thermal carriers (e.g., phonon) on the C sample becomes shorter due to its high void fraction. In contrast, the metallic spacers tend to fill up some voids and to create a conductive carbon-metal network, thus, enhancing the thermal transport efficiency.

To support this argument, the void fractions are determined based on the evaluation of apparent densities of all carbon composites. The void fractions are 32, 36, 44, and 76% for CAl, CNi, CSn, and C samples, respectively. It is obvious that the void fraction is significantly reduced by the insertion of metallic spacers. Moreover, the apparent densities of CAl, CNi, CSn, and C samples are measured to be 1.33, 1.11, 0.85, and 0.72 g/cm^3, respectively. As expected, the metallic spacer serves as not only as filler but also as connective point for creating additional path for heat conduction. Therefore, the metal-coated carbon composites provide a well-developed thermal conductive skeleton, leading to high-efficiency thermal diffusion. It is worth noting that the CAl sample displays the highest *k* value among all carbon heat sinks. The improved performance can be attributed to the fact that the CAl sample possesses the lower void fraction, as compared to the others. The observation is well identical with the analysis of N_2 physisorption. Accordingly, the Al_2O_3 spacers are believed to be effectively inserted into the carbon-based infrastructure, forming thermally conductive framework. Thus, the unique framework (i.e., CAl heat sink) is capable of exhibiting the enhanced thermal conduction efficiency due to well-developed thermal pathway and low void fraction.

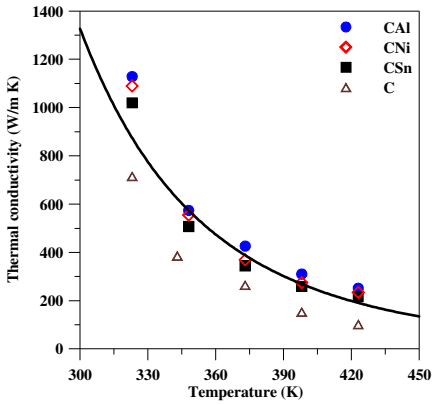

Fig. 10 The relationship between in-plane thermal and electrical conductivity of carbon samples.

The relationship between the σ value and the apparent *k* value for all samples is depicted in Fig. 10, in which all readings were obtained from the measurements at 50°C. The figure clearly shows that the apparent *k* value is an increasing function of σ value within the entire experimental range. It is well known that the electronic transport strongly depends on the thermal case, dominated by lattice vibration and phonon transport.[19,20] This result observed from Fig. 10 also confirms the above deduction that the conduction of free electrons in conductors is analogous to the thermal transport. This finding delivers useful information regarding thermal conduction and heat dissipation efficiencies of carbon-based composites, facilitating the design of thermal devices, e.g., heat sink and heat exchanger. On the basis of experimental results, the selection of metallic spacers and weight loading could play a crucial role in tuning the thermal transport and electrical conduction efficiencies of heat sinks.

Conclusions

The present work has revealed an improved thermal transport efficiency of metal-coated carbon composites, as compared to pristine carbon. Three types of metallic nanoparticles including Al_2O_3, Ni, and SnO were employed as spacers to insert into the carbon black powder, forming well-developed carbon framework. An increase of 42.5–57.7 % in the improved *k* value was attained after the introduction of metallic spacers. The CAl sample at 50°C exhibited the highest *k* value of 1128 W/m K as compared with the other carbon samples. The metallic spacers serve as not only as fillers but also as connective points for creating additional path for the heat conduction. Thus, the metal-coated carbon composites provide a well-developed thermal conductive skeleton, leading to highly-efficient thermal diffusivity. Additionally, the apparent k value as an increasing function of σ value could be

found within the entire experimental range. This result demonstrated that the conduction of free electrons in conductors is analogous to the thermal transport. The present work provided useful information concerning the thermal conduction and heat dissipation efficiencies of carbon-based composites, benefiting the design of thermal devices, e.g., heat sink and heat exchanger. The design of metal-coated carbon heat sinks has a commercial potential to replace costly metal-based heat sinks due to its facile preparation, good chemical stability, and low thermal expansion.

Acknowledgements

The authors are very grateful for the financial support from the Ministry of Science and Techonology (Taiwan) under the contract MOST 103-2221-E-155-014-MY2.

References

1 Q. Wang, X. H. Han, A. Sommer, Y. Park, C. T'Joen, A. Jacobi, *Int. J. Refrig*, 2012, **35**, 7-26.
2 G. Yuan, X. Li, Z. Dong, A. Westwood, Z. Cui, Y. Cong, H. Du, F. Kang, *Carbon*, 2012, **50**, 175-182.
3 R. Sengupta, M. Bhattacharya, S. Bandyopadhyay, A. K. Bhowmick, *Prog. Polym. Sci*., 2011, **36**, 638-670.
4 Z. Liu, Q. Guo, J. Shi, G. Zhai, L. Liu, *Carbon*, 2008, **46**, 414-421.
5 J. C. Bokros, *Chemistry and physics of carbon, vol. 5*, 1969, 97-103.
6 S, Zhou, J. Xu, Q. H. Yang, S. Chiang, B. Li, H. Du, C. Xu, F. Kang, *Carbon*, 2013, **57**, 452-459.
7 Q. Liang, Y. Xuxia, W. Wang, Y. Liu, C. P. Wong, *ACS Nano*, 2011, **5**, 2392–2401.
8 P. Goli, H. Ning, X. Li, C. Y. Lu, *Nano Lett*., 2014, **14**, 1497–1503.
9 J. Haskins, A. Kınacı, C. Sevik, H. Sevinçli, G. Cuniberti, T. Çağın, *ACS Nano*, 2011, **5**, 3779–3787.
10 C. T. Hsieh, C. E. Lee, Y. F. Chen, J. K. Chang, H. Teng, *Nanoscale*, 2015, **7**, 18663–18670.
11 L. Yanga, J. Chenb, N angd, B. Li, *Int. J. Heat Mass Transfer*, 2015, **91**, 428–432.
12 S. Zhou, J. Xu, Q. H. Yang, S. Chiang, B. Li, H. Du, C. Xu, F. Kang, *Carbon*, 2013, **57**, 452–459.
13 Q. M. Gong, Z. Li, Y. Wang, B. Wu, Z. hang, J. Liang, *Mater. Res. Bull*., 2007, **42**, 474–481.
14 C. W. Huang, C. H. Hsu, P. L. Kuo, C. T. Hsieh, H. Teng, *Carbon*, 2011, **49**, 895-903.
15 G. Wang, X. Shen, J. Yao, J. Park, *Carbon*, 2009, **47**, 2049-2053.
16 E. Pop, D. Mann, Q. Wang, K. Goodson, H. Dai, *Nano Lett*., 2006, **6**, 96–100.
17 S. Berber, Y. K. Kwon, D. Tomanek, *Phys. Rev. Lett*., 2000, **84**, 4613–4616.
18 S. Iijima, *Nature*, 1991, **354**, 56–58.
19 M. Zhou, H. Bi, T in, X. Lü, D. Wan, F. Huang, J. Lin, *Carbon*, 2014, **75**, 314–321.
20 P. Keblinski, S. Phillopt, S. Choi, J. Eastman, *Int. J. Heat Mass Transfer*, 2002, **45**, 855–863.